Exchange coupling and natural ferromagnetic resonance phenomena in $Fe_{40}Co_{37}Zr_{11}N_{12}/ZrN/Ni_{80}Fe_{20}$ film systems with in-plane uniaxial anisotropy

K. Seemann

Karlsruhe Institute of Technology KIT (Campus North), Institute for Applied Materials, Hermann-von-HelmholtzPlatz 1, 76344 Eggenstein-Leopoldshafen, Germany

Keywords:
Ferromagnetic films
Exchange coupling
Magnetic polarisation
In-plane uniaxial anisotropy
FMR
Precession damping
Spin currents

A B S T R A C T

Ferromagnetic $Fe_{40}Co_{37}Zr_{11}N_{12}/ZrN/Ni_{80}Fe_{20}$ film systems with a uniaxial anisotropy in the film plane were synthesised by reactive magnetron sputtering and by post annealing in a static magnetic field. Investigation on the energy exchange interaction between the ferromagnetic layers without and with an interface layer were carried out. This exchange impacts the static magnetisation properties as well as the natural resonance frequency behaviour and its damping features caused by spin current generated damping and/or anti-damping effects. As static polarisation loops are slightly but distinguishably different dependent on the interface thickness, the films definitely exhibit a distinct variation in their frequency spectra. By means of the interface layer with different thickness, various dynamic behavioural patterns could be observed. This can be assumed because the observed ferromagnetic resonance dual lines show remarkable changes in their full width at half maxima (FWHM) at frequencies of around 600 MHz attributed to the $Ni_{80}Fe_{20}$ layers and 2.3 GHz attributed to the $Fe_{40}Co_{37}Zr_{11}N_{12}$ layers if interface layer are applied.

1. Introduction and motivation

The nature of single films has been studied with regard to many aspects like polarisation behaviour according to micro- and domain structure, magnetic anisotropy as well as shape in the nanometre regime. Beside these static features, investigations on their high-frequency behaviour are still an ongoing branch of research. Due to the fact, that these films are quite easy to fabricate they are suitable for, e.g., micro inductors, micro transducers or for settling EMC issues. Additional activities on ferromagnetic films for contactless stress or torque measurements are under way and promise an interesting and hot-topic area of research for sensor applications [1–4].

Today, the diversity of applications for ferromagnetic thin films promotes intensive research activities, and therefore, it demands a variety of film materials. Currently, non-ferromagnetic materials, i.e. conducting, semiconducting, superconducting as well as insulating films in combination with ferromagnetic films are in the focus of spintronics, as generally known, since the discovery of the GMR effect [5,6]. This lead to components like read/write heads in hard discs, GMR sensors and MRAMS for storage systems. Here, fast switching of the magnetic spins or moments is predominantly a challenge, which especially floats questions of high interest concerning the origin of damping mechanisms. Damping is generated during the ferromagnetic resonance frequency absorption by losses or perturbation of magnetic spin precession where electromagnetic energy is converted into, e.g. imperceptible heat. The resonance frequency peaks are more or less broad, and they are a magnitude of probability at which frequency energy is absorbed at most. Hence, damping mechanisms like intrinsic damping by Zeeman transition, 3d itinerant magnetic electrons which interact with phonons (spin–orbit coupling) causing spin flip, extrinsic damping by two-magnon scattering processes and spin sink phenomena (spin flip) in non-ferromagnetic interface layers have to be analysed and, if needed, minimised by an appropriate film microstructure design, composition and film architecture [7,8]. If these films are exposed to an electromagnetic wave they come up with impressive high-frequency properties. While the static properties are touched by an exchange interaction energy [9,10] the high-frequency behaviour is affected by a spin transfer torque due to spin currents which generates a positive or negative contribution to precession damping [11–13].

The present paper just aims at these features and intends to feel out spin current effects in trilayer systems, i.e. for a metallic-like ZrN interface layer with higher resistivity and ferromagnetic film materials with clearly different magnetisation and uniaxial anisotropy values. ZrN is also used due to its good were resistance properties, but it is still a

E-mail address: klaus.seemann@kit.edu.

conducting material with an appropriate spin diffusion length. $Fe_{40}Co_{37}Zr_{11}N_{12}$ as a ferromagnetic nanocomposite film material is sufficient in terms of a high saturation magnetisation, thermal stability, i.e. inhibited grain growth while being exposed to higher temperatures, and herewith, it stays soft magnetic through a negligible magneto-crystalline anisotropy similar to $Ni_{80}Fe_{20}$. In contrary to $Ni_{80}Fe_{20}$, the $Fe_{40}Co_{37}Zr_{11}N_{12}$ nanocomposite provides a magnetostrictive behaviour, which generates some change in magnetoelastic energy. Nevertheless, it provides a marked in-plane uniaxial anisotropy after thermal conditioning as an important requirement for frequency suitability [14]. This combination of features and combined with $Ni_{80}Fe_{20}$, this trilayer system now forms a new object of study for technically applicable systems like alternative magnetoelastic sensor concepts for which a stress induced ferromagnetic resonance frequency shift can be a measure of mechanical torque [4]. The paper focuses its attention on the nature of the frequency features being a crucial factor for optimising thin film torque sensor applications, and it looks inside of damping by discussing spin transfer torque in these trilayer systems, in order to optimise frequency spectra for appropriate signal-to-noise ratio exploitation.

2. Theoretical considerations of a trilayer system

2.1. Ferromagnetic polarisation behaviour

If a trilayer thin film system (non-ferromagnetic interface layer with thickness t_{int} between two different ferromagnetic film materials with thickness t_{m1} and t_{m2} (Ferromagnet1/Non-Ferromagnet/Ferromagnet2 (F1/N/F2)) is exposed to a magnetic field the polarisation loops must be described in a more complex way. The usual approach for it is to find the energy balance of the entire film system. By neglecting the magneto-crystalline anisotropy, which tends to a minimum value due to the chemical composition and nanometre grain size, the total free energy per unit area of the sandwich system can generally be established. By taking an in-plane uniaxial anisotropy and the Stoner-Wohlfarth criteria [15] into account, the energy possesses the following form,

$$\begin{aligned} E_f \quad & \{K_{u1}\cdot(1 \quad cos^2\varphi_1)\cdot t_{m1}+K_{u2}\cdot(1 \quad cos^2\varphi_2)\cdot t_{m2}\} \\ & \{\mu_0\cdot M_{s1}\cdot H_{ext}\cdot cos(\beta_1 \quad \alpha_H)\cdot t_{m1} \\ & +\mu_0\cdot M_{s2}\cdot H_{ext}\cdot cos(\beta_2 \quad \alpha_H)\cdot t_{m2}\} \\ & J_{ex1}\cdot\cos(\beta_1 \quad \beta_2) \quad J_{ex2}\cdot cos^2(\beta_1 \quad \beta_2) \end{aligned} \tag{1}$$

The terms in the first curly bracket represent the uniaxial anisotropy energies with their anisotropy coefficients K_{u1} and K_{u2} of the first and second ferromagnetic layer, respectively. The second curly bracket defines the Zeeman energies which include the magnetic field constant μ_0, the saturation magnetisation M_{s1} and M_{s2} as well as the external in-plane magnetic field H_{ext} with an angle α_H relative to the x-direction. The last two empirical terms stand for the exchange coupling interaction which is characterised by the common bilinear J_{ex1} and the biquadratic J_{ex2} coupling parameters [9,10,16].

Furthermore, we assume that F1 and F2 are ferromagnetic materials with different magnetisation as well as in-plane uniaxial anisotropies. By placing the polarisation J_s $\mu_0\cdot M_s$ it is useful to write the anisotropy coefficients as K_u $\frac{1}{2}\cdot J_s\cdot H_u\cdot(1 \quad cos^2\varphi)$ which now contain directly measurable magnitudes. At zero external field a saturated polarisation state is assumed in the film plane in z-direction due to the anisotropy field H_{ui} (i 1, 2).

Consequently, one can set $\varphi_i \approx \beta_i$, and Eq. (1) turns into

$$\begin{aligned} E_f \quad & \frac{1}{2}\cdot\{J_{s1}\cdot H_{u1}\cdot(1 \quad cos^2\beta_1)\cdot t_{m1}+J_{s2}\cdot H_{u2}\cdot(1 \\ & cos^2\beta_2)\cdot t_{m2}\} \quad \{J_{s1}\cdot H_{ext}\cdot cos(\beta_1 \quad \alpha_H)\cdot t_{m1} \\ & +J_{s2}\cdot H_{ext}\cdot cos(\beta_2 \quad \alpha_H)\cdot t_{m2}\} \quad J_{ex1}\cdot\cos(\beta_1 \quad \beta_2) \\ & J_{ex2}\cdot cos^2(\beta_1 \quad \beta_2) \end{aligned} \tag{2}$$

In order to obtain the J-H_{ext} polarisation behaviour, Eq. (2) is minimised according to β_1 and β_2 which constitutes the equilibrium polarisation state in relation to the external magnetic field. If once the angles are determined at the energy minimum, the polarisation can be similarly defined according to [17]. We additionally postulate that a resultant saturation polarisation of the triple layer systems can be formed by the individual saturation polarisation of the first (J_{s1}) and second (J_{s2}) ferromagnetic layer and its corresponding thickness,

$$J_s \quad \frac{J_{s1}\cdot t_{m1}+J_{s2}\cdot t_{m2}}{t_{m1}+t_{m2}} \tag{3}$$

The polarisation contribution of the individual layers in dependence on the external magnetic field are J_1 $J_{s1}\cdot sin\beta_1$ and J_2 $J_{s2}\cdot sin\beta_2$, respectively. Finally, the shape of the overall external magnetic field-dependent polarisation, neglecting domain wall motion as well as coercive fields, can now be numerically computed by equation

$$J(H_{ext},\beta_1,\beta_2) \quad \frac{J_{s1}\cdot t_{m1}+J_{s2}\cdot t_{m2}}{t_{m1}+t_{m2}}\cdot\frac{J_{s1}\cdot sin\beta_1\cdot cos(\beta_1 \quad \alpha_H)+J_{s2}\cdot sin\beta_2\cdot cos(\beta_2 \quad \alpha_H)}{J_{s1}\cdot sin\beta_1+J_{s2}\cdot sin\beta_2} \tag{4}$$

By means of Eq. (4), it is possible to investigate the shape of the polarisation curves as well as the in-plane uniaxial anisotropy relations and the exchange coupling parameters at the energy minimum mentioned above which can be found in (2). If the polarisations J_{s1} and J_{s2} are parallel J_{ex1} possesses a positive value, and they are antiparallel if J_{ex1} is negative. In the case for which the biquadratic coupling parameter J_{ex2} dominates, J_{s1} and J_{s2} are perpendicular to each other. Let us assume that the magnetic moments of both ferromagnetic layers are in plane J_{ex2} is quite small, i.e., the biquadratic energy exchange in (2) is almost ineffective.

2.2. Dynamic features

In consideration of the transversal in-plane high-frequency field the ferromagnetic moments precess about their direction they are forced to by the in-plane uniaxial anisotropy.

This can be clearly shown by the frequency-dependent permeability, which is described by means of the modified Landau-Lifschitz-Gilbert (LLG) differential equation [18] in combination with the Maxwell equation [19]. The Maxwell equation characterises possible eddy-current generation in the film, but it tends to be small if the film is appropriately thin. While the magnetic moments excitation results in magnetic spin precession, intrinsic damping mechanisms like spin–orbit coupling, and usually extrinsic damping by two-magnon scattering generation, influences the shape of the ferromagnetic frequency spectrum. Spin currents emitted by the individual magnetic layers are responsible for additional damping which is in focus of the upcoming dynamic investigations. The following schemes of the F1/N/F2 trilayer film with two different ferromagnetic film materials with individual ferromagnetic resonance frequencies illustrates their architecture and sketches the spin current mechanisms if the film system is exposed to a high-frequency electromagnetic wave (Fig. 1(a)–(c)).

Due to the fact that thin ferromagnetic films are considered ($t_m <$ 100 nm) where eddy-currents can be nearly excluded we are able to consider an extended version of the pure LLG's dynamic characterisation for which one usually applies the bilinear static interaction J_{ex1} between the ferromagnetic layers [20]. But for an on-resonance layer and for a weak static exchange coupling we neglect the interaction term here and are primarily interested in the additional damping parameter α_{spi} which is correlated with the spin currents between the ferromagnetic layers [21,22]. Then, one writes the dynamic LLG equation in a more simple form,

$$\frac{\partial\vec{M}_i}{\partial t} \quad \gamma_i\cdot\vec{M}_i\times H_{effi}+\frac{(\alpha_{Gi}+\alpha_{spi})}{M_{si}}\cdot\vec{M}_i\times\frac{\partial\vec{M}_i}{\partial t} \tag{5}$$

in which one finds the effective field associated with the extended and

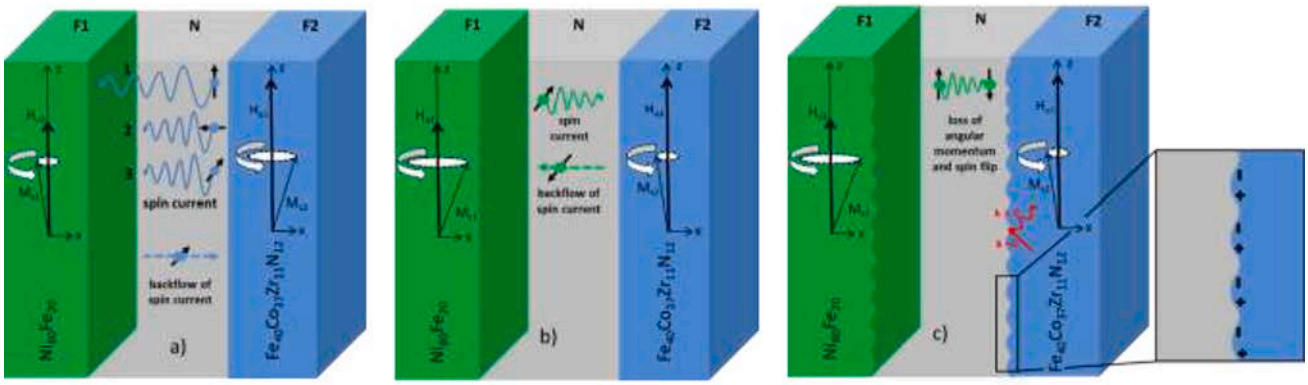

Fig. 1. Illustration of the film architecture Ferromagnet1/Non-Ferromagnet/Ferromagnet2 (F1/N/F2). In (a), there is a spin current (1 longitudinal flow || M_s, 2 and 3 transverse flow ⊥ M_s) and backflow of spin current emitted by the $Fe_{40}Co_{37}Zr_{11}N_{12}$ layer which is on resonance. In (b), it is the inverse path if the $Ni_{80}Fe_{20}$ layer is on resonance and (c) exhibits spin flip and two-magnon scattering ($k = 0 \rightarrow k > 0$) as well as fluctuations in the magnetic order due to the "orange-peel" demagnetising effect for high interface layer thickness. The thickness of all layers is not to scale.

exact natural ferromagnetic resonance frequency (FMR) formula according to [23]

$$f_{FMRi} \quad \frac{\gamma_i}{2\pi \cdot \left(1 + \left(\alpha_{Gi} + \alpha_{spi}\right)^2\right)} \cdot \mu_0 \cdot H_{effi}$$

$$\frac{\gamma_i}{2\pi \cdot \left(1 + \left(\alpha_{Gi} + \alpha_{spi}\right)^2\right)} \cdot \mu_0 \cdot \sqrt{H_{ui}^2 + H_{ui} \cdot M_{si}} \quad \left(\alpha_{Gi} + \alpha_{spi}\right) \frac{M_{si}^2}{4} \tag{6}$$

So, two individual resonances for each layer (labelled by the index i) are expected. α_{Gi} is the Gilbert damping parameter of the single layer, and the damping parameter due to additional spin pumping which causes a spin transfer torque is described by α_{spi}. It can be positive or negative in sign. As a result, the total damping to be analysed, while neglecting two-magnon scattering for a magnetic film thickness of a few tens nm, is

$$\alpha_i^{tot} \quad \alpha_{Gi} + \alpha_{spi} \tag{7}$$

Two-magnon generation, i.e., degenerate $k > 0$ magnons are "not allowed" [7] or at least are reduced in a way that they do not affectively appear [8], but assuming low two-magnon scattering for a constant magnetic films thickness of 50 nm, it would not obviously change the results due to a very small offset. This can fairly be assumed for an almost perfect layer architecture.

Now, it is convenient to take possession of the full width at half maximum (FWHM) of the imaginary part of the frequency-dependent permeability spectrum Δf_{FMRi}, in order to obtain information about the damping behaviour of the film stack. By making use of the analytical relation between the FWHM and the damping parameter according to [24] we are reasonably able to calculate α_{spi} from expression (7) in a range of $\Delta f_{FMRi} < 1$ GHz. The associated formula to be considered for the determination, whether $\alpha_{spi} < 0$ or $\alpha_{spi} > 0$, now is

$$\Delta f_{FMRi} \quad \frac{\gamma_i}{2\pi} \cdot \left(J_{si} + \mu_0 \cdot H_{ui}\right) \cdot \left(\alpha_{Gi} + \alpha_{spi}\right) \tag{8}$$

Substituting α_{Gi} by

$$\alpha_{Gi} \quad \frac{2\pi}{\gamma_i} \cdot \frac{\Delta f_{sri}}{\left(J_{si} + \mu_0 \cdot H_{ui}\right)} \tag{9}$$

and solving Eq. (8) for α_{spi} the spin current damping parameter can be expressed as

$$\alpha_{spi} \quad \frac{2\pi}{\gamma_i \cdot \left(J_{si} + \mu_0 \cdot H_{ui}\right)} \cdot \left(\Delta f_{FMRi} \quad \Delta f_{sri}\right) \tag{10}$$

In the formula we find γ_i the gyromagnetic parameter and Δf_{sri} the FWHM of the i^{th} film material of the single layers. The FWHMs are directly quantifiable from the measured frequency spectra.

3. Experimental methods

Soft (F1/N/F2) triple layer $Fe_{40}Co_{37}Zr_{11}N_{12}$/ZrN/$Ni_{80}Fe_{20}$ nanocomposite films were deposited on oxidised Si (1 0 0) substrates (1 μm silicon oxide, dim. 5 mm × 5 mm × 0.375 mm) by reactive r.f. magnetron sputtering in an Ar/N_2 atmosphere (except $Ni_{80}Fe_{20}$) all at a constant pressure of 0.5 Pa. The argon/nitrogen gas flow fraction for $Fe_{40}Co_{37}Zr_{11}N_{12}$ and ZrN was kept constant at about 70 sccm/1 sccm. For deposition, 6-inch targets (target composition in at.-%: $Fe_{42}Co_{41}Zr_{17}$, ZrN, $Ni_{80}Fe_{20}$) were used in a Leybold Heraeus Z550 sputtering device. The sputtering power for all targets was 250 W. Three samples of each single layer and trilayer combination, i.e., 30 samples were fabricated, in order to verify the reproducibility of properties and to support the estimation of error bars. The thickness of the films were measured by means of a TENCOR P-10 Surface Profiler by scanning a sharp edge between a coated and uncoated area on a flat Si substrate. Thickness was additionally determined by the exact sputtering rate. As a result, the ferromagnetic layers varied merely a few nanometres and were determined to be close around 50 nm each. The interface layer thickness was determined by using the sputtering rate and confirmed by exemplarily measuring an entire film stack. Finally, roughness plays a role in the polarisation and high-frequency behaviour. For higher interface thickness, the roughness adds up to approximately 9 nm (R_a). The fact that the Profiler resolution is reached and roughness for the thinner interfaces could not be resolved, roughness can be assumed to be lower than 9 nm in these films.

During an annealing process at 400 °C for 2 h in a static magnetic field of around 50 mT an in-plane uniaxial anisotropy was induced. The polarisation loop $J(\mu_0 H_{ext})$ of the easy and hard direction of the magnetic polarisation was measured by means of a QD VersaLab vibrating sample magnetometer (VSM), in order to obtain the saturation polarisation J_{si} of the single ferromagnetic layers and the trilayer systems as well as the uniaxial anisotropy fields $\mu_0 \cdot H_{ui}$. The high-frequency permeability measurements were carried out with a strip-line permeameter designed for frequencies up to 5 GHz [25,26] which is connected to an Agilent 8753 ES network analyser.

4. Experimental results

4.1. The static and dynamic magnetic characteristic of the $Ni_{80}Fe_{20}$ and $Fe_{40}Co_{37}Zr_{11}N_{12}$ single films

The single films exhibit an induced in-plane uniaxial anisotropy $\mu_0 \cdot H_{ui}$ which is estimated between 0.3 and 0.6 mT for the $Ni_{80}Fe_{20}$ film

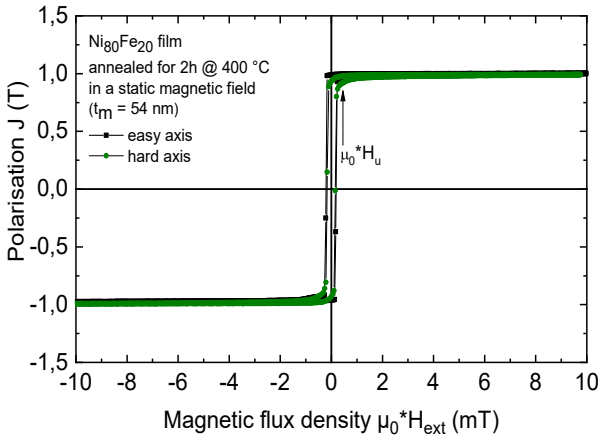

Fig. 2. Hard and easy axis polarisation loops of a single $Ni_{80}Fe_{20}$ film 54 nm in thickness which was annealed at 400 °C for 2 h in an external static magnetic field. The arrow indicates the approximate uniaxial anisotropy field.

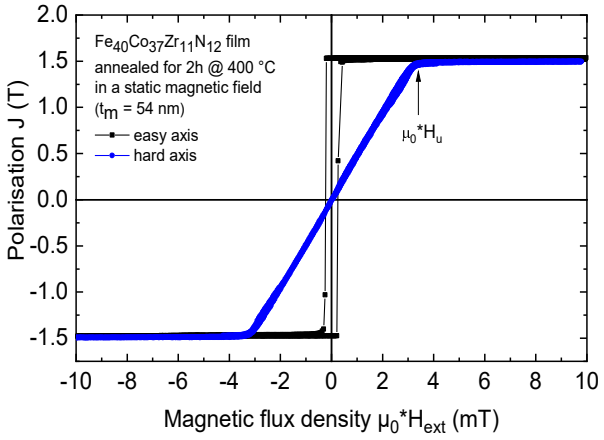

Fig. 3. Hard and easy axis polarisation loops of a single $Fe_{40}Co_{37}Zr_{11}N_{12}$ film 54 nm in thickness which was annealed at 400 °C for 2 h in an external static magnetic field. The arrow indicates the approximate uniaxial anisotropy field.

(Fig. 2) and around 3.0–4.0 mT for the $Fe_{40}Co_{37}Zr_{11}N_{12}$ film (Fig. 3). They possess a thickness of around 54 nm. The saturation polarisations J_{si} are 1 T and 1.5 T, respectively. As expected, a soft ferromagnetic behaviour, i.e. a coercive field below 1 mT could be observed due to the film composition and the nanocomposite ($Fe_{40}Co_{37}Zr_{11}N_{12}$) as well as nanocrystalline structure. Regarding the polarization loops one can see very defined and clear hard and easy axes which exhibit a very soft magnetization.

Especially, $Ni_{80}Fe_{20}$ provides an excellent magnetic softness due to its extremely low magnetocrystalline anisotropy. Considering its saturation polarisation of around 1 T it is comparable to those which can be found in [27,28], but may slightly vary at different sputtering parameters. After conditioning the individual formation of iron and nickel to chains of short-range order generates the in-plane uniaxial anisotropy and does not really impact the magnetic saturation. Conditioning delivers anisotropy values which can also be compared to those mentioned in literature.

The film material $Fe_{40}Co_{37}Zr_{11}N_{12}$ bares a higher magnetic saturation and in-plane uniaxial anisotropy. First, Fe-Co-Zr-N films, and as a single work, were introduced in [29] but have never been continued. In their research paper, the saturation polarisation nearly represents a value close to that depicted in the present paper. The uniaxial anisotropy was somewhat different, i.e. higher by trend due to divergent compositions. In [14,8], Fe-Co-Zr-N films were picked up again and investigated and discussed under quantum mechanical and spin dynamic aspects, e.g., how the formation of ferromagnetic transition elements leads to an in-plane uniaxial anisotropy through thermal treatment in a static magnetic field.

By virtue of the elaborated composition $Fe_{40}Co_{37}Zr_{11}N_{12}$ the films show a soft magnetic behaviour. This originates from its Fe-Co nanocrystallites for which the magnetocrystalline anisotropy is minimised predominantly by grain size but has a stronger pseudo-dipole interaction generating uniaxial anisotropy than $Ni_{80}Fe_{20}$. The reduction of grain growth is caused by a second diffusion inhibiting stoichiometric and thermally stable ZrN phase, also called grain growth reducer. This could be shown by the author, elsewhere, and was discussed in some publications of related film materials containing Hf-N. HfN possesses the same enthalpy of formation, i.e. 360 kJ/mol, like ZrN.

All these static properties fulfil the qualification for a suitable frequency response of magnetic moments. The conditions for the natural ferromagnetic resonance are now provided by the fact that the films behave as being uniformly magnetised due to their marked uniaxial anisotropy. So, no external field is necessary, in order to saturate the magnetic moments. Hence, a uniform, coherent precession of the magnetic electrons or moments is performed. This is shown by means of the natural ferromagnetic resonance spectra presented by the frequency-dependent permeability. According to the uniaxial anisotropies and saturation polarisations the FMR amounts to about f_{FMR} 547 MHz for the $Ni_{80}Fe_{20}$ film (Fig. 4) and f_{FMR} 2.3 GHz for the $Fe_{40}Co_{37}Zr_{11}N_{12}$ film (Fig. 5). An initial permeability μ_r ($f \rightarrow 0$) of about 1830 and 250 could be observed, respectively. It is conspicuous that the dynamic features can be well described by the LLG theory (according to Eq. (5)).

Due to the fact, that the measured spectra perfectly coincide with the LLG theory and the ferromagnetic resonances frequencies correspond to the calculated values an assumed uniform magnetisation state is justified. Consequently, to use an external field is not necessary and can be neglected in Eq. (6).

Relating the frequency spectrum of $Ni_{80}Fe_{20}$ to [30] one can observe that the frequency characteristics can be reproduced. Due to its pronounced soft magnetic disposition the weak uniaxial anisotropy field can hardly be overlapped by a magnetocrystalline anisotropy which would cause fatal damping and perturbation of the uniform precession of magnetic moments. As a result, the FWHM of 0.361 GHz and the corresponding damping parameter α_{Gi} of around 0.017 can be confirmed by [30,31], but it can also be lower in some cases where different high-frequency measurement techniques were used or discrepancies in stoichiometry and variation in microstructure could be denoted by certain coating parameters [32].

The FWHM of $Fe_{40}Co_{37}Zr_{11}N_{12}$ amounts to 0.241 GHz and possesses

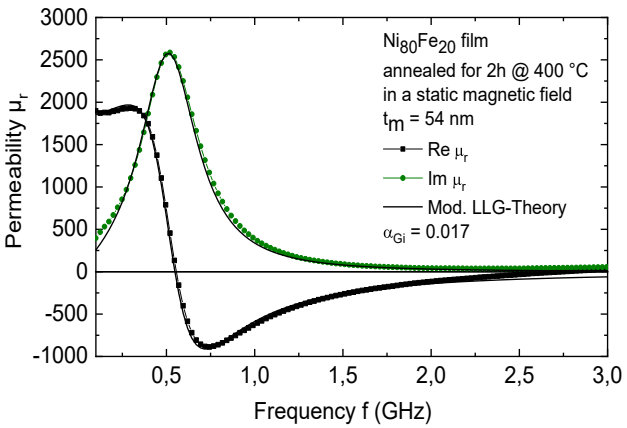

Fig. 4. Real- and imaginary part of the frequency-dependent permeability of a single $Ni_{80}Fe_{20}$ film with a thickness of 54 nm. The solid curve represents the modified LLG theory and is in a good agreement with the experimental data. For calculation, a gyromagnetic constant γ of 175 GHz/T was assumed.

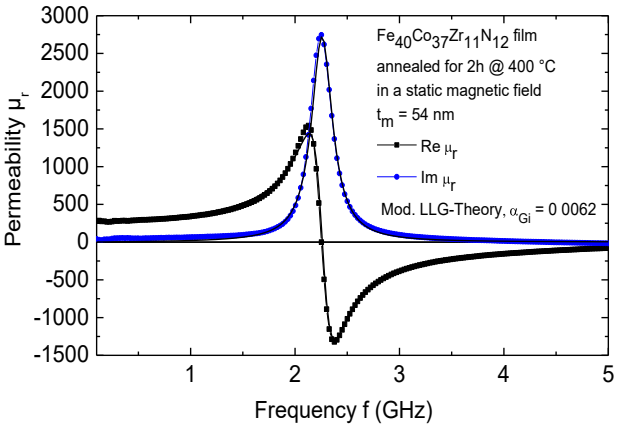

Fig. 5. Real- and imaginary part of the frequency-dependent permeability of a single $Fe_{40}Co_{37}Zr_{11}N_{12}$ film with a thickness of 54 nm. The solid curve represents the modified LLG theory and is in a good agreement with the experimental data. For calculation, a gyromagnetic constant γ of 180 GHz/T was assumed.

a damping parameter of 0.0062, which reproducibly match the same film material system in [8,14] and similar ferromagnetic film materials [33,34].

4.2. The static and dynamic magnetic characteristic with ZrN interface layer of various thickness

4.2.1. The ferromagnetic $Fe_{40}Co_{37}Zr_{11}N_{12}/Ni_{80}Fe_{20}$ bilayer film

Starting with a non-interface bilayer the two magnetic materials reveal an observable exchange interaction (Fig. 6). This results into an ordinary hysteresis loop exhibiting an in-plane uniaxial anisotropy field of about 2.2 mT and a saturation polarisation of 1.3 T which is apparently different in comparison to each single film material. By applying Eq. (4) for the simulation of the polarisation curve one can demonstrate that the double layer pretends to be a "homogeneous" material. The saturation polarisation could be verified according to the postulated expression (3), and the in theory resulting in-plane uniaxial anisotropy comparably confirmed the measured data by the numerical calculation (4) with an approximate minimum coupling parameter of J_{ex1} $3.0 \cdot 10^{-4}$ J/m^2. The interaction exchange energy empirically reaches a large positive value, which keeps the magnetic moments of both different magnetic film materials in a parallel ferromagnetic direction. The resulting in-plane uniaxial anisotropy, determined by the hard and easy axis polarisation loops, approximately results in the arithmetic average of the two anisotropy fields of the single films, which is also confirmed by the theoretic calculation.

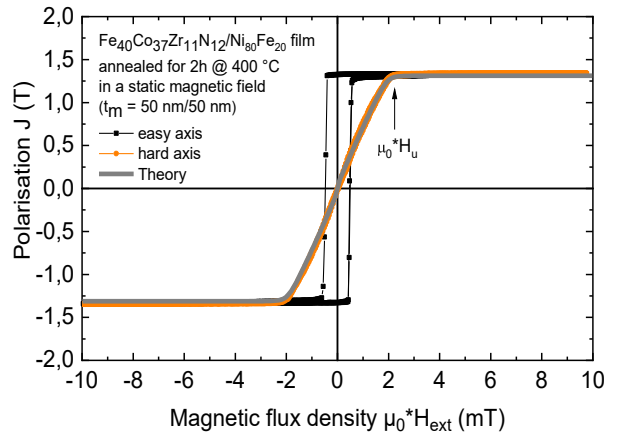

Fig. 6. Hard and easy axis polarisation loops of a $Fe_{40}Co_{37}Zr_{11}N_{12}/Ni_{80}Fe_{20}$ double layer film 50 nm, each layer in thickness, which was annealed at 400 °C for 2 h in an external static magnetic field. The arrow indicates the uniaxial anisotropy field. The grey solid curve shows the theoretical polarisation behaviour of the hard axis according to (4).

Obviously, the strong interaction energy J_{ex} generates an exchange coupling field which causes one in-plane uniaxial anisotropy. At this point, we assume a parallel alignment of the distinct magnetic moments which results in a common switching process. The frequency-dependent permeability shows one resonance peak at about 1.5 GHz which conclusively reflects the static magnetic features (Fig. 7).

As expected, the frequency spectrum behaves according to the magnetic polarisation features and sufficiently reflects the resulting in-plane uniaxial anisotropy and saturation polarisation field. The bilayer merely exhibits one resonance maximum presented by the imaginary part of the permeability. Due to the strong direct interaction J_{ex} only one single resonance maximum appears.

If $Ni_{80}Fe_{20}$ is on resonance it generates a spin current into the adjacent $Fe_{40}Co_{37}Zr_{11}N_{12}$ layer and induces off-resonance precession by means of spin transfer torque. It is demonstrative that the resonance peak shows a FWHM of 0.331 GHz which is lower than that of the single $Ni_{80}Fe_{20}$ film but a bit higher than that of the single $Fe_{40}Co_{37}Zr_{11}N_{12}$ film. So, there is an effective damping process by spin torque, i.e., beside the intrinsic Gilbert damping (bulk damping), transverse spin currents impact the resonance precession by anti-damping and additional damping, respectively.

4.2.2. The static and dynamic magnetic characteristic of $Fe_{40}Co_{37}Zr_{11}N_{12}$/ZrN/$Ni_{80}Fe_{20}$ triple layer films

Now, we turn to an interface layer ZrN which possesses a finite resistivity in the range of 10^{-5} and 10^{-6} Ohm·m [35,36]. The values depend on the thermal treatment and sputtering conditions. A different static and dynamic performance could be observed by employing a ZrN interface layer.

Just from 1 nm (3 to 4 monolayers) interface layer thickness yet, the hard axis of polarisation is differently shaped in comparison to the latter case. The polarisation measurements signify that now two individual in-plane uniaxial anisotropies can be resolved within the hard axis J-H_{ext} loops (Fig. 8(a)–(c)) which approximately coincide with the anisotropies found for the single films. One can observe two implied slopes of the hard axis loops, so it is obvious that the exchange interaction energy is much weaker than for the double layer arrangement. Although, the exchange energy is low, it still causes interaction between the ferromagnetic layers. The theoretical verification with J_{ex1} $3.6 \cdot 10^{-5}$ J/m^2, J_{ex2} 0 J/m^2 for 1 nm, J_{ex1} $3.0 \cdot 10^{-5}$ J/m^2; J_{ex2} $1.2 \cdot 10^{-5}$ J/m^2 for 10 nm and J_{ex1} $2.8 \cdot 10^{-5}$ J/m^2, J_{ex2} $1.3 \cdot 10^{-5}$ J/m^2 for the 100 nm interface layer confirms the observed polarisation behaviours. It

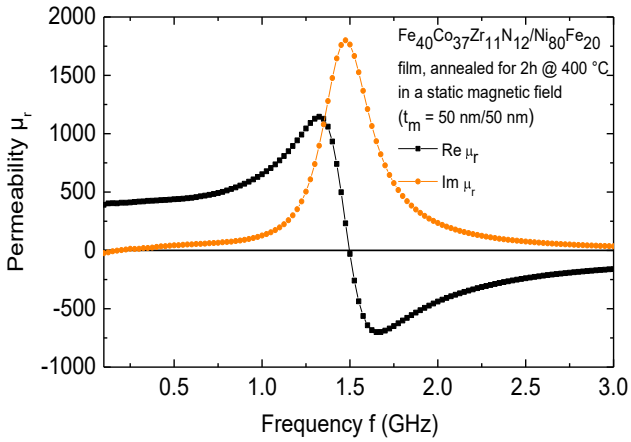

Fig. 7. Real- and imaginary part of the frequency-dependent permeability of a $Fe_{40}Co_{37}Zr_{11}N_{12}/Ni_{80}Fe_{20}$ double layer film, each layer 50 nm in thickness.

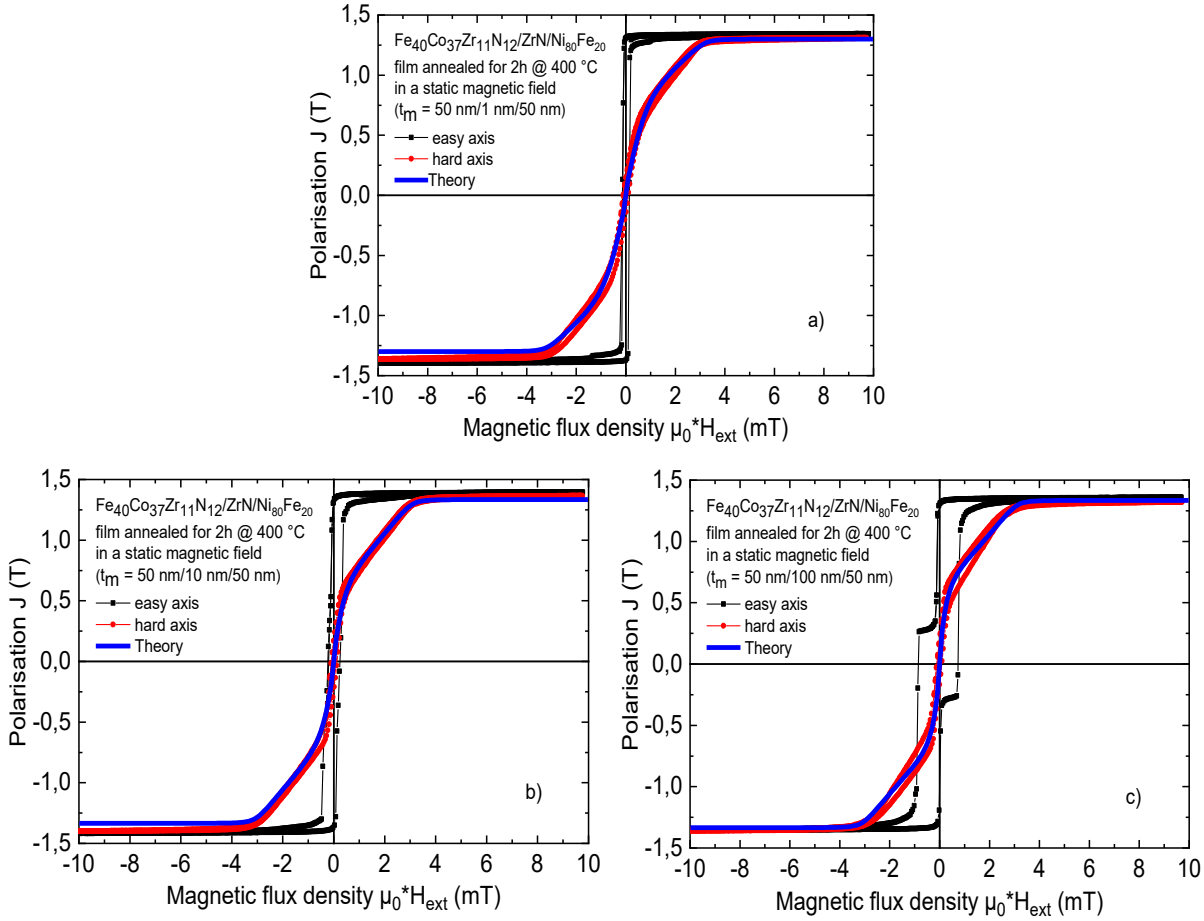

Fig. 8. Hard and easy axis polarisation loops of $Fe_{40}Co_{37}Zr_{11}N_{12}/ZrN/Ni_{80}Fe_{20}$ trilayer layer films which were annealed at 400 °C for 2 h in an external static magnetic field. The films possess a thickness of (a) 50 nm/1 nm/50 nm, (b) 50 nm/10 nm/50 nm and (c) 50 nm/100 nm/50 nm, respectively. The thick solid lines in blue show the theoretical polarisation behaviour of the hard axis according to (4).

is conspicuous that biquadratic exchange appears which may be the origin of beginning surface roughness at a higher interlayer thickness. This can result into magnetic frustration, i.e. perturbation of the ferromagnetic order. Considering the theory the two slopes explain the small exchange energy parameters, i.e. the interaction between the ferromagnetic layers is so weak, so that the magnetic moments rotate nearly independently.

J_{ex} is varied as a fitting parameter in the formulas (1)–(4), in order to describe the magnetic polarisation. This is just visible in the hard direction of polarisation. Although, the exchange energy parameters are low they are still present and affect the hard axis of polarisations as shown by the fitted theory. In Fig. 8c, it is noticeable that two kinks can be observed in the easy axis of polarisation. Here, the magnetic moments suddenly seem to switch in two steps. It seems probable that higher roughness at 100 nm interface layer thickness ($R_a \approx 9$ nm) leads to this behaviour by pinning magnetic moments or microscopic demagnetisation effects, the so-called “orange-peel” effect. Here, the magnetic softness can slightly suffer from the perturbation of the magnetic order. Additionally, one can be sure that dipolar coupling between the magnetic layers due to roughness can be definitely excluded. By estimating the dipolar energy at 100 nm interface layer thickness [37] its value varies in the range of $1 \cdot 10^{-10}$ to $1 \cdot 10^{-20}$ J/m^2 for an assumed periodicity of roughness between 50 and 20 nm.

In face of the small exchange interaction energy the permeability spectra stand out by two separate resonance maxima which are in agreement with the in-plane uniaxial anisotropies (Fig. 9(a)–(c)). So, exchange is not effectual to generate one resonance state, but it is conspicuous that the FWHMs of the two resonance peaks change on the dependence of the interface layer thickness t_{int}. In Fig. 10, one can observe that the FWHM increases after reaching a minimum at around 25 nm assigned to $Ni_{80}Fe_{20}$ and at 50 nm assigned to $Fe_{40}Co_{37}Zr_{11}N_{12}$. Due to changes of the FWHM one can assume that the angular momentum of the ferromagnetic layers is transferred into their conduction bands (s-d exchange) and injected into the interface layer which mutually influences the damping behaviour of the individual ferromagnetic layers.

From varying FWHMs, one can deduce a spin current (spin transfer from the ferromagnetic layer into the nonmagnetic interface layer conduction band with reduced states via s-d interaction) which changes in the dependence on the interlayer thickness. Both Δf_{FMRi} differ from their corresponding Δf_{sri} with lower FWHM ($Ni_{80}Fe_{20}$) or with a higher FWHM ($Fe_{40}Co_{37}Zr_{11}N_{12}$) for thin ZrN interface layers between 1 and 5 nm before reaching a minimum at 30 and 50 nm, respectively, until they approach the nominal Δf_{sri} between 90 and 100 nm interface layer thickness. By consideration of Eq. (10), and assuming sheer Gilbert damping α_{Gi} gained from the bare single layers, the damping parameter α_{spi} reveals the range of damping and anti-damping processes (Fig. 11). Up to approximately 10 nm ZrN, $Ni_{80}Fe_{20}$ is a spin sink for $Fe_{40}Co_{37}Zr_{11}N_{12}$ due to loosing angular moment by scattering and absorption with zero backflow of transverse spin moments to the on-resonance $Fe_{40}Co_{37}Zr_{11}N_{12}$ layer. This means there is no spin accumulation at the $ZrN/Ni_{80}Fe_{20}$ interface, but for $Ni_{80}Fe_{20}$ anti-damping, described by negative α_{spi}, can be observed in a wide range. Both α_{spi} are different in sign below 10 nm interface layer thickness because the different ferromagnetic film materials have different spin splits due to their different anisotropy states. From around 10 nm ZrN on, α_{spi}

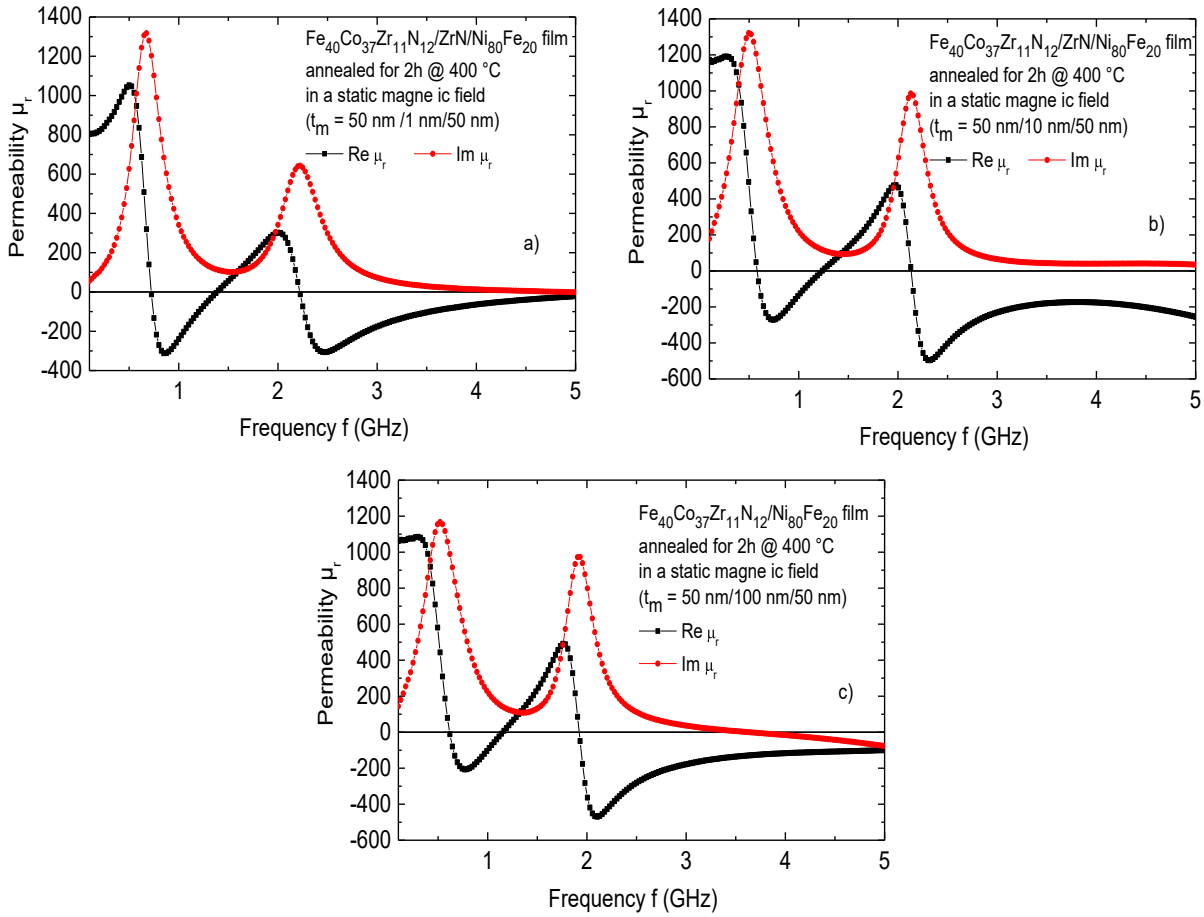

Fig. 9. Real- and imaginary part of the frequency-dependent permeability of $Fe_{40}Co_{37}Zr_{11}N_{12}$/ZrN/$Ni_{80}Fe_{20}$ trilayer layer films. The individual layers possess a thickness of (a) 50 nm/1 nm/50 nm, (b) 50 nm/10 nm/50 nm and (c) 50 nm/100 nm/50 nm, respectively.

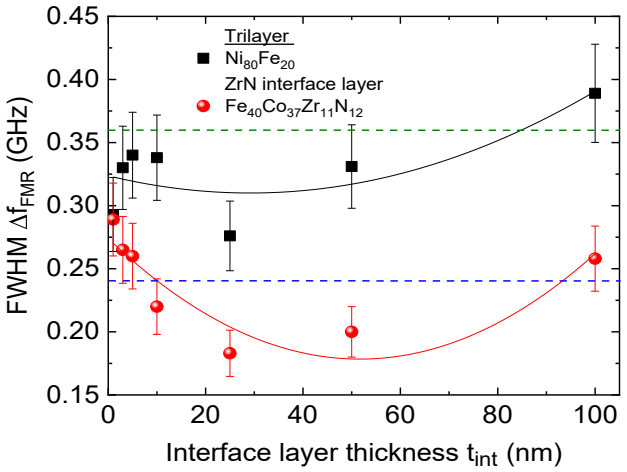

Fig. 10. Full width at halve maximum of the imaginary part of the frequency-dependent permeability of $Fe_{40}Co_{37}Zr_{11}N_{12}$/ZrN/$Ni_{80}Fe_{20}$ trilayer layer films dependent on the ZrN interface layer thickness. The dashed horizontal lines indicate the FWHM of the single films. The solid curve is a guide to the eye for the data points. The error bars indicate an uncertainty of 10%.

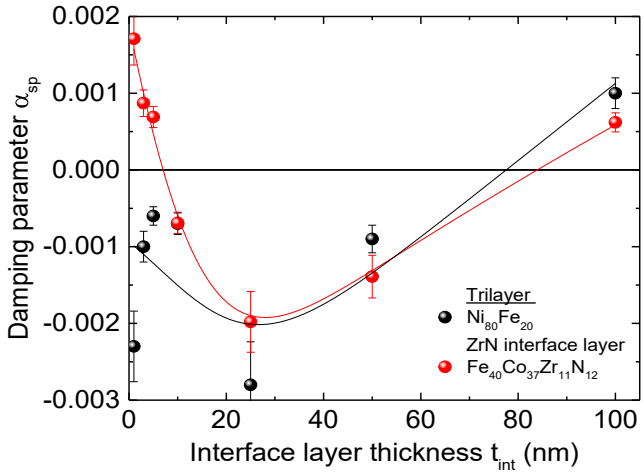

Fig. 11. Damping parameter α_{spi} of the $Fe_{40}Co_{37}Zr11N_{12}$/ZrN/$Ni_{80}Fe_{20}$ trilayer layers dependent on the interface layer thickness, t_{int}. The error bars indicate an uncertainty of 10%.

assigned to $Fe_{40}Co_{37}Zr_{11}N_{12}$ also becomes negative. Just for an interface thickness between 10 and 20 nm the backflow mechanism may dominate and both ferromagnetic layers experience a negative α_{sp}, i.e., accelerating torque is supported.

If the interface layer is too thick and the two resonances are still separated, pumping of spins across a nonmagnetic layer is commonly suppressed. As the spin current gradually decays and cannot reach the second ferromagnetic layer, loss of angular momentum and backflow into the respective on-resonance layer is present. This can produce simultaneous damping as well as anti-damping. If anti-damping dominates due to less scattering in a certain range of interface layer thickness

both ferromagnetic films can show a negative α_{sp}. From the range of 20 nm to 30 nm interface thickness, even now the majority spins, which travel much further than minority spins, loose more and more angular momentum due to higher thickness. Additionally, the interface layer thickness becomes higher than the spin flip length of between 20 and 60 nm for ZrN, which can be estimated by the electronic band structure properties [38]. This results in more damping while spin pumping increasingly reduces, and there is less backflow of magnetic moments into the individual on-resonance layers. From about 80 nm ZrN thickness damping exceeds the single layer values of both ferromagnetic film materials. Due to the fact, that roughness at the interfaces has presumably increased more fluctuation in the magnetic order perturbs spin precession, which results in more damping, i.e. inhomogeneous broadening. Roughness even causes scattering centres where two-magnon generation arises. It is assumed that the strong increase of broadening is a combination of two-magnon and ordinary or spin flip scattering, so one is not able to distinguish between static exchange-, spin current effects and effects originating from perturbation of the precessing ferromagnetic spin system.

In Fig. 12, the ferromagnetic resonance field is plotted vs. the interface layer thickness.

It can be observed that the resonance field of the $Fe_{40}Co_{37}Zr_{11}N_{12}$ layer slightly decreases for higher interface layer thickness whereas the resonance field of $Ni_{80}Fe_{20}$ nearly remains constant. Approaching 100 nm interface layer thickness the resonance field of $Fe_{40}Co_{37}Zr_{11}N_{12}$ clearly deviates from its single film value. This seems obvious because the increasing roughness at the interface leads to some perturbation of the uniaxial anisotropy field by the already mentioned "orange-peel effect". Microscopic magnetic dipoles (Fig. 1c) arise by local demagnetisation and generate local magnetic fields which counteract the uniaxial anisotropy field across the layer thickness. Obviously, this effect is somewhat more pronounced at the proximity of the $Fe_{40}Co_{37}Zr_{11}N_{12}$/ZrN junction. This effect can also be observed for Co/Ni multilayer systems with Cu buffer layers [39], for which roughness lowers, although slightly, the anisotropy, i.e. the resonance field. Additionally, it increases inhomogeneous broadening due to reasons already discussed.

5. Conclusion

The present paper highlights the static and dynamic properties (natural ferromagnetic resonance) of trilayer systems with different ferromagnetic film materials separated by a ZrN interface layer. It could be demonstrated that those film systems can be used to influence or manipulate their static and high-frequency properties. The polarisation measurements showed that there is a weak exchange interaction between the layers. As analysis has shown a common coupling parameter J_{ex1} dominates, which may be attributed to RKKY interaction, at least for interface layers of some nm in thickness. Even dipole interaction between the ferromagnetic layers can be an option for interaction due to roughness because it should be in the same order of magnitude. At higher interface layer thickness it is more difficult to select between coupling effects of the magnetic layers. For higher interface layer thickness, dipole interaction can be certainly excluded because its energy drops exponentially. Concerning the high-frequency features, spin currents affect precession damping which influences the natural ferromagnetic resonance FWHM, which can be higher or lower than their individual FWHM as single layers. This reflects the total damping parameter, which is reduced or enhanced. At higher interface layer thickness damping is apparently dominated by perpetuation effects like two magnon-scattering and fluctuation of magnetic moments, i.e. inhomogeneous broadening in addition to Gilbert damping.

With regard to applications, especially where low damping plays a decisive role, the manipulation of dynamic properties of ferromagnetic/non-ferromagnetic film stacks can be realised. Dependent on and by controlling the interface layer thickness total damping is reduced below the nominal Gilbert bulk damping value.

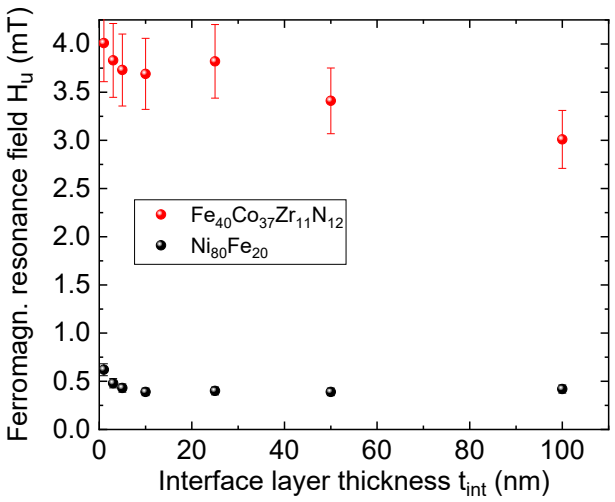

Fig. 12. Ferromagnetic resonance field in dependence on the interface layer thickness. The error bars indicate an uncertainty of 10%. The resonance field is determined by solving Eq. (6) for H_u.

CRediT authorship contribution statement

K. Seemann: Conceptualization, Data curation, Formal analysis, Funding acquisition, Investigation, Methodology, Project administration, Resources, Software, Supervision, Validation, Visualization, Writing - original draft, Writing - review & editing.

Declaration of Competing Interest

The authors declare that they have no known competing financial interests or personal relationships that could have appeared to influence the work reported in this paper.

References

[1] C. Bechtold, I. Teliban, C. Thede, S. Chemnitz, E. Quandt, Sens. Actuators A 158 (2010) 224.
[2] K. Krüger, K. Seemann, H. Leiste, M. Stüber, S. Ulrich, J. Magn. Magn. Mater. 343 (2013) 42.
[3] K. Seemann, S. Beirle, C. Thede, V. Schier, E. Quandt, Sens. Actuator A Phys. 296 (2019) 278.
[4] S. Beirle, K. Seemann, Sens. Actuator A Phys. 301 (2020) 111788.
[5] M.N. Baibich, J.M. Broto, A. Fert, F. Nguyen Van Dau, F. Petroff, P. Eitenne, G. Greuzet, A. Friederrich, J. Chazelas, Phys. Rev. Lett. 61 (1988) 2472.
[6] G. Binasch, P. Grünberg, F. Saurenbach, W. Zinn, Phys. Rev. B 39 (1989) 4828.
[7] C.E. Patton, C.H. Wilts, F.B. Humphrey, J. Appl. Phys. 38 (1967) 1358.
[8] K. Seemann, S. Beirle, H. Leiste, J. Phys. D: Appl. Phys. 50 (2017) 405001.
[9] S. Demokritov, A. Wolf, P. Grünberg, Europhys. Lett. 15 (1991) 881.
[10] P. Grünberg, S. Demokritov, A. Fuss, R. Schreiber, J.A. Wolf, S.T. Purcell, J. Magn. Magn. Mater. 104–107 (1992) 1734.
[11] B. Heinrich, Y. Tserkovnyak, G. Woltersdorf, A. Brataas, R. Urban, G.E.W. Bauer, Phys. Rev. Lett. 90 (2003) 187601–187611.
[12] T. Taniguchi, H. Imamura, Phys. Rev. B 76 (2007) 092402.
[13] D.C. Ralph, M.D. Stiles, J. Magn. Magn. Mater. 320 (2008) 1190.
[14] K. Seemann, S. Beirle, H. Leiste, J. Magn. Magn. Mater. 413 (2016) 115.
[15] E.C. Stoner, E.P. Wohlfarth, Philos. Trans. R Soc. Lond. Ser. A (1948) 240 599.
[16] A. Layadi, Phys. Rev. B 65 (2002) 104422.
[17] M. Belmeguenai, T. Martin, G. Woltersdorf, M. Maier, G. Bayreuther, Phys. Rev. 76 (2007) 104414.
[18] T.L. Gilbert, IEEE Trans. Magn. 40 (2004) 3443.
[19] K. Seemann, H. Leiste, V. Bekker, J. Magn. Magn. Mater. 278 (2004) 200.
[20] A.A. Baker, A.I. Figueroa, D. Pingstone, V.K. Lazarov, G. van der Laan, T. Hesjedal, Sci. Rep. 6 (2016) 35582.
[21] A.A. Baker, A.I. Figueroa, L.J. Collins-McIntyre, G. van der Laan, T. Hesjedal, Sci. Rep. 5 (2015) 7907.
[22] A.I. Figueroa, A.A. Bake, L.J. Collins-McIntyre, T. Hesjedal, G. van der Laan, J. Magn. Magn. Mater. 400 (2016) 178.
[23] K. Seemann, H. Leiste, K. Krüger, *Magn. Res. Solids* Electron. J. 16 (2014) 14301.
[24] K. Seemann, H. Leiste, C. Klever, J. Magn. Magn. Mater. 321 (2009) 3149.
[25] V. Bekker, K. Seemann, H. Leiste, J. Magn. Magn. Mater. 270 (2004) 327.
[26] Y. Liu, L. Chen, C.Y. Tan, H.J. Liu, C.K. Ong, Rev. Sci. Inst. 76 (2005) 063911.

[27] A.-M. Nguyen, S. Cercelaru, G. Tremblay, J.-C. Perron, P. Hesto, Thin Solid Films 275 (1996) 231.
[28] J.P. Nibarger, R. Lopusnik, Z. Celinski, T.J. Silva, Appl. Phys. Lett. 83 (2003) 93.
[29] K. Nakanishi, O. Shimizu, S. Toshida, IEEE Trans. Magn. 27 (1991) 5322.
[30] O. Archer, S. Queste, M. Ledieu, Phys. Rev. B 68 (2003) 184414.
[31] G.M. Sandler, H.N. Bertram, T.J. Silva, T.M. Crawford, J. Appl. Phys. 85 (1999) 5080.
[32] S. Ingvarsson, L. Ritchie, X.Y. Liu, G. Xiao, J.C. Slonczewski, P.L. Trouilloud, R. H. Koch, Phys. Rev. B 66 (2002) 214416.
[33] Y. Liu, Z.W. Liu, C.Y. Tan, C.K. Ong, J. Appl. Phys. 100 (2006) 093912.
[34] K. Seemann, H. Leiste, K. Krüger, J. Magn. Magn. Mater. 345 (2013) 36.
[35] A. Rizzo, M.A. Signore, D. Valerini, D. Altamura, A. Cappello, L. Tapfer, Surf. Coat. Technol. 206 (2012) 2711.
[36] S. Khan, M. Mehmood, I. Ahmad, F. Ali, A. Shah, Mater. Sci. Semicond. Process. 30 (2015) 486.
[37] J.C.S. Kools, W. Kula, J. Appl. Phys. 85 (1999) 4466.
[38] P. Marksteiner, P. Weinberger, A. Neckel, R. Zeller, P.H. Dederichs, J. Phys. F: Met. Phys. 16 (1986) 1495.
[39] J.M. Shaw, H.T. Nembach, T.J. Silva, J. Appl. Phys. 108 (2010) 093922.